

Descriptors for Hydrogen Evolution on Single Atom Catalysts in Nitrogen-Doped Graphene

Published as part of *The Journal of Physical Chemistry virtual special issue "Machine Learning in Physical Chemistry"*.

Victor Fung,[#] Guoxiang Hu,[#] Zili Wu, and De-en Jiang*



Cite This: *J. Phys. Chem. C* 2020, 124, 19571–19578



Read Online

ACCESS |



Metrics & More

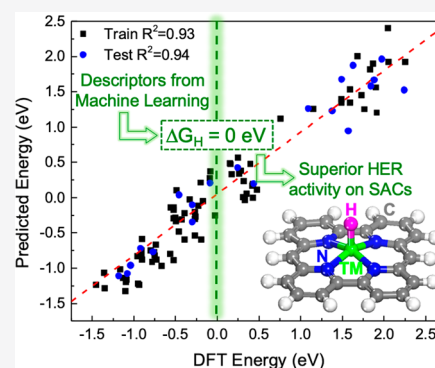


Article Recommendations



Supporting Information

ABSTRACT: Single-atom catalysts (SACs) are a new research frontier in electrocatalysis such as in the hydrogen evolution reaction (HER). Recent theoretical and experimental studies have demonstrated that certain M–N–C (metal–nitrogen–carbon) based SACs exhibit excellent performance for HER. Here we report a new approach to tune HER activity for SACs by changing the size and dimensionality of the carbon substrate while maintaining the same coordination environment. We screen the 3d, 4d, and 5d transition metal SACs in N-doped 2D graphene and nanographenes of several sizes for HER using first-principles density functional theory (DFT). Nanographenes containing V, Rh, and Ir are predicted to have significantly enhanced HER activity compared to their 2D graphene counterparts. We turn to machine learning to accurately predict the free energy of hydrogen adsorption (ΔG_{H}) based on various descriptors and compressed sensing to identify key descriptors for activity, which can be used to further screen for additional candidates.



INTRODUCTION

To reduce the use of fossil fuels and mitigate global warming, significant attention has been turned to the use of hydrogen as a renewable fuel.¹ Water splitting is an ideal way of hydrogen production which can utilize electricity from renewable energy. A major obstacle hampering the application of this catalytic process is the need to find stable, cost-effective, and earth abundant catalysts to replace precious metals such as Pt, which are currently among the most efficient catalysts for hydrogen evolution reaction (HER).² Metal compounds such as nitrides, phosphides and sulfides have shown promise in recent years for this reaction.^{3–9} In addition, 2D materials such as transition metal dichalcogenides^{10–14} and graphene-supported metal atoms^{15–18} have also been demonstrated to be viable catalysts.

Transition metal single atom catalysts (SACs) on graphene offer a number of appealing benefits such as a 100% metal utilization, high activity, and broad tunability in chemical properties. Graphene represents a suitable stable and highly conducting substrate with high surface area to support the single atoms, which can be further tuned by the doping of elements such as nitrogen to improve performance. These single atoms generally are found in the single or double vacancy of the pristine or N-doped graphene support, which can be stabilized by three or four M–C or M–N covalent bonds.^{19,20} They have been widely studied and characterized in recent years for various applications including HER, but the underlying design principles and properties governing their

catalytic activity remain under intense study. The performance of these SACs is hypothesized to depend on the chemical bonding and charge transfer between atomically dispersed metal and substrate materials.^{21–23}

To tune the catalytic performance of SACs on graphene, approaches via changing the SAC element, the coordination environment of the SAC, and substrate doping (by primarily S, P, and N atoms) have been tried.²⁴ Beyond the nonmetal doping of the graphene, varying the substrate size (i.e., from 2D periodic graphene to nanographene molecules of varying size) offers a hereto unexplored path toward a more precise and controllable approach of tuning the substrate electronic structure. Moreover, single atoms in macrocycles have been shown to be stable and can serve as active molecular catalysts from prior experimental studies.^{25,26} Modulating properties of SACs via the substrate electronic structure²⁷ is a promising approach, and we adopt it here to examine the HER activity of SACs by changing a metallic graphene substrate to a macrocyclic or nanographene substrate with molecule-like states. We subsequently screen the 3d, 4d, and 5d transition

Received: May 17, 2020

Revised: August 7, 2020

Published: August 12, 2020



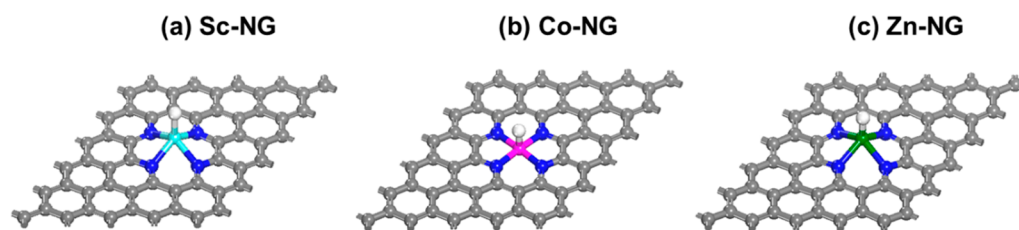


Figure 1. Optimized structures of H adsorption on the transition-metal single atom embedded on N-doped graphene (NG): (a) Sc-NG, (b) Co-NG, (c) Zn-NG. Key: C, gray; N, blue; H, white; Sc, cyan; Co, magenta; Zn, green.

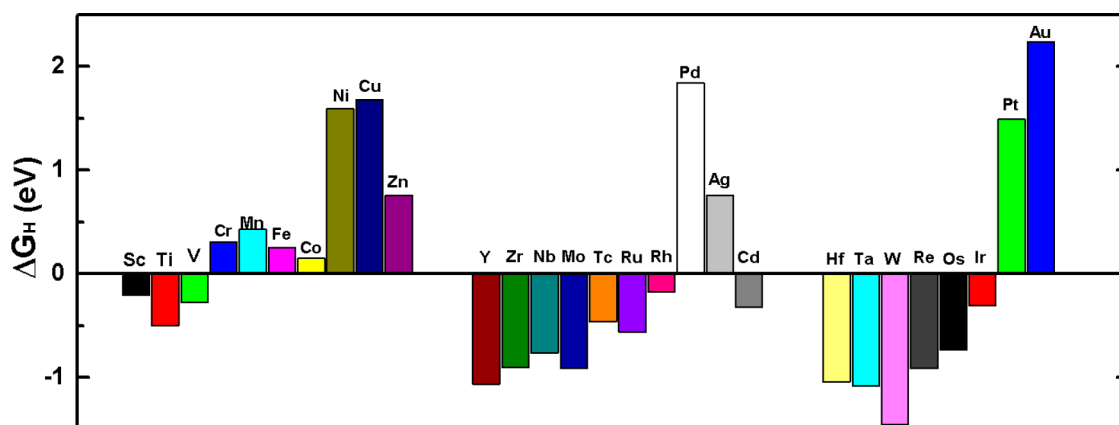


Figure 2. Computed ΔG_H for 3d, 4d, and 5d transition-metal single atoms embedded in N-doped graphene.

metal (TM) atoms embedded in the substrate via the Gibbs free energy of H adsorption (ΔG_H) obtained from first-principles density functional theory (DFT). Then, we use machine-learning approaches to correlate some key descriptors to the HER activity.

■ COMPUTATIONAL METHODS

Spin-polarized density functional theory (DFT) calculations were performed using the Vienna *ab initio* simulation package (VASP).^{28,29} Electron exchange-correlation was represented by the functional of Perdew, Burke, and Ernzerhof (PBE) of generalized gradient approximation (GGA).³⁰ The ion-electron interaction was described with the projector augmented wave (PAW) method.³¹ The plane-wave cutoff is set to 400 eV, and a conjugate gradient method is applied to relax the geometry until interatomic forces are less than 0.025 eV/Å.

The SACs supported on nitrogen-doped graphene were modeled by 5×6 graphene super cells containing 54 carbon atoms. A vacuum of 20 Å along the z -direction was employed for the 2D N-doped graphene monolayer, which is periodic in the xy -plane. The Brillouin zone was sampled by $(3 \times 3 \times 1)$ Monkhorst–Pack k -point mesh.

The SACs supported on N-doped nanographenes of different sizes were modeled in cubic boxes ($30 \text{ Å} \times 30 \text{ Å} \times 30 \text{ Å}$), each containing one SAC at the center of a N-doped-nanographene. The large, medium, and small N-doped nanographenes contain 102, 56, and 22 carbon atoms, respectively. The Γ point only was used to sample the k space.

The H adsorption energy ΔE_H was calculated by $\Delta E_H = E(\text{catalyst} + \text{H}) - E(\text{catalyst}) - \frac{1}{2}E(\text{H}_2)$, where $E(\text{catalyst} + \text{H})$ represents the total energy of the catalyst with one adsorbed H atom, $E(\text{catalyst})$ represents the total energy of the catalyst, and $E(\text{H}_2)$ represents the total energy of a gas phase H_2 molecule. The Gibbs free energy of H adsorption, ΔG_H ,

was obtained by $\Delta G_H = \Delta E_H + \Delta E_{ZPE} - T\Delta S_H$, where ΔE_{ZPE} is the difference in zero-point energy between the adsorbed H and H in the gas phase H_2 molecule, and ΔS_H is the entropy difference between the adsorbed H and $\frac{1}{2}\text{H}_2$ in the gas phase under standard conditions. The zero-point energy was calculated by summing vibrational frequencies ω over normal modes ν : $E_{ZPE} = \frac{1}{2} \sum \hbar\omega$. The entropy of the free H_2 molecule at 298.15 K and 1 atm was taken from the NIST database.³² The formation energy E_f of the SAC was calculated by $E_f = E(\text{catalyst}) - E(\text{substrate}) - E(\text{TM})$, where $E(\text{substrate})$ represents the total energy of the N-doped graphene and $E(\text{TM})$ represents the total energy of the atomic transition metal. A negative value of E_f suggests a favorable formation.

Machine learning models were applied using methods implemented in the Scikit-learn Python package.³³ In the machine learning fitting, the 80% of the data for training (and the rest 20% for testing) were selected randomly from the full data set (in Table S1) using a standard sci-kit learn function in python. The training and test include a sampling of all possible elements in the four substrates, in order to train for adsorption across the different adsorbates. The data were preprocessed first via standard scaling. For kernel ridge regression, a polynomial kernel was used with degree = 2 and gamma = 0.1. For random forest regression, the max depth was set to 3. For the neural network regression, two hidden layers of size 25 were used with the ReLU activation function. Compressed sensing was further performed with sure independence screening and sparsifying operator (SISSO).³⁴

■ RESULTS AND DISCUSSION

Screening of TM Embedded in N-Doped Graphene as SACs for HER. The Volmer step leading to H adsorption is the first step of HER.^{35,36} Since the Gibbs free energy for

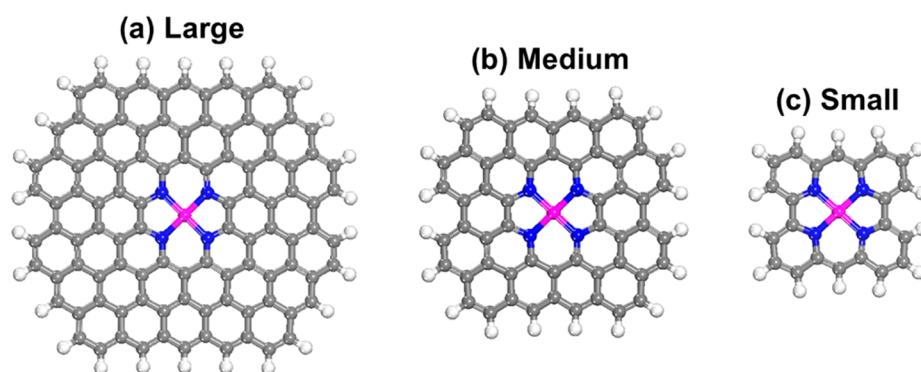


Figure 3. Structures of single transition-metal atoms embedded in N-doped nanographenes of different sizes: (a) large, (b) medium, and (c) small. Key: C, gray; H, white; N, blue; metal, magenta.

hydrogen adsorption (ΔG_{H}) is a well-established descriptor for HER in many catalytic materials,³⁷ we examine H adsorption at 3d, 4d, and 5d single TM atoms embedded in N-doped graphene (NG) by computing ΔG_{H} . The optimized geometries of H adsorption at single TM atoms embedded in NG are illustrated in Figure 1. H is found to preferentially adsorb at the top site of the TM atoms. For the majority of SACs, the TM atoms are found to be situated in-plane to the graphene both before and after H adsorption, such as Co–NG (Figure 1b). However, the early and late transition metals, specifically the group 3 and group 12 elements, are found to be out-of-plane, such as Sc–NG (Figure 1a) and Zn–NG (Figure 1c). This can be attributed to the larger radius of the early TM and the weaker metal–nitrogen interaction of the late TM with NG.

We show the ΔG_{H} in Figure 2 and can see some interesting trends. First, the H adsorption is most negative on the early transition metals and becomes weaker (more positive) from left to right within each period. There is a dramatic uphill change in H adsorption energy from group 9 to group 10, which results in highly unfavorable H adsorption on the group 10 and 11 transition-metal atoms. Second, H adsorption becomes stronger down each group (e.g., Cr to Mo to W), particularly in groups 3 (Sc–Y) to 9 (Co–Rh–Ir), a trend that has been observed in other SAC systems as well.³⁸

The obtained adsorption free energies in Figure 2 are consistent with previously reported ΔG_{H} of SACs in N-doped graphene from DFT-PBE,^{22,23} and in the present work, we have sampled more SAC elements. We note that ΔG_{H} values may vary with functional (e.g., for Y@N₄ SAC²³); here, our focus is on the overall trends. Furthermore, the best predicted HER catalyst based on ΔG_{H} , Co on N-doped graphene (Co–NG), had been synthesized and shown to have high HER performance in several recent experimental studies by others,^{22,39} validating our computational method. Other promising catalysts with ΔG_{H} close to zero are predicted to be Sc, V, Fe, Rh, and Ir in NG. We did not include Cd as a promising catalyst since the formation energy for the Cd SAC is much less negative than other SACs (E_{f} in Table S1), indicating that it is much less stable.

Tuning HER Activity with Size of Graphene. Figure 2 shows that ΔG_{H} can vary quite dramatically from one element to the next and spans an energy range of over 3 eV for the TM SAC on NG. To further tune ΔG_{H} toward zero, we systematically explored the size effect of the graphene substrate on ΔG_{H} . Three successively smaller hydrogen-terminated N-doped nanographenes were considered: large, 102 carbon

atoms (Figure 3a); medium, 56 carbon atoms (Figure 3b); small, 22 carbon atoms (Figure 3c).

Figure 4 compares SACs embedded in the three different sizes of N-doped nanographenes and those in the extended N-

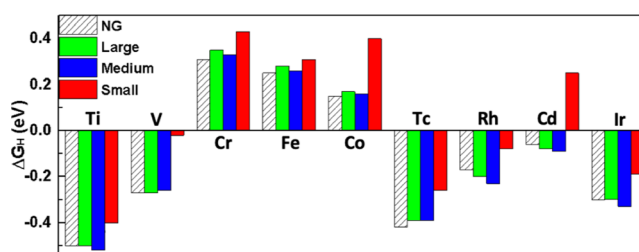


Figure 4. Comparison of ΔG_{H} for single transition-metal atoms embedded in N-doped graphene (NG) and N-doped nanographenes of different sizes.

doped graphene; only the SACs whose ΔG_{H} values are within -0.5 to 0.5 eV are shown. We find no major changes in ΔG_{H} for the large and medium N-doped nanographenes but a significant weakening of H binding (by 0.1 – 0.3 eV) for the small ones. As shown previously, a difference of 0.3 eV for ΔG_{H} can alter the exchange current density j_0 , or rate, by 3 orders of magnitude.^{11,40} For SACs which overbind the hydrogen (with more negative ΔG_{H}) when in extended NG, such as Ti, V, Tc, Rh, and Ir, we predict that their HER performance will be improved when they are embedded in the small N-doped nanographene (SNNG), which is essentially a macrocyclic ligand for the SAC center. In particular, V–SNNG was found to have a ΔG_{H} of -0.03 , which is closer to zero than any of the previously studied SACs, including Co–NG. We note that Tc is radioactive; we included it just for the sake of comparison with other SACs.

To understand the origin of the weaker H adsorption on SACs embedded in SNNG, we analyzed the center of their d-states (Table S1) and found a downshift in comparison with that on 2D N-doped graphene for some SACs. For example, as shown for V in Figure 5, one can clearly see that V d-states in N-doped graphene (Figure 5a) shift down in the small nanographene (Figure 5b); the d-band center shifts from 1.32 eV for the former to 0.44 eV for the latter. The downshift could be attributed to a stronger interaction between the V SAC and the small nanographene as the formation of stronger covalent bonds between the V SAC and the graphene leads to hybridized states which are lower in energy. There is a greater degree of hybridization between the SAC and carbon in the

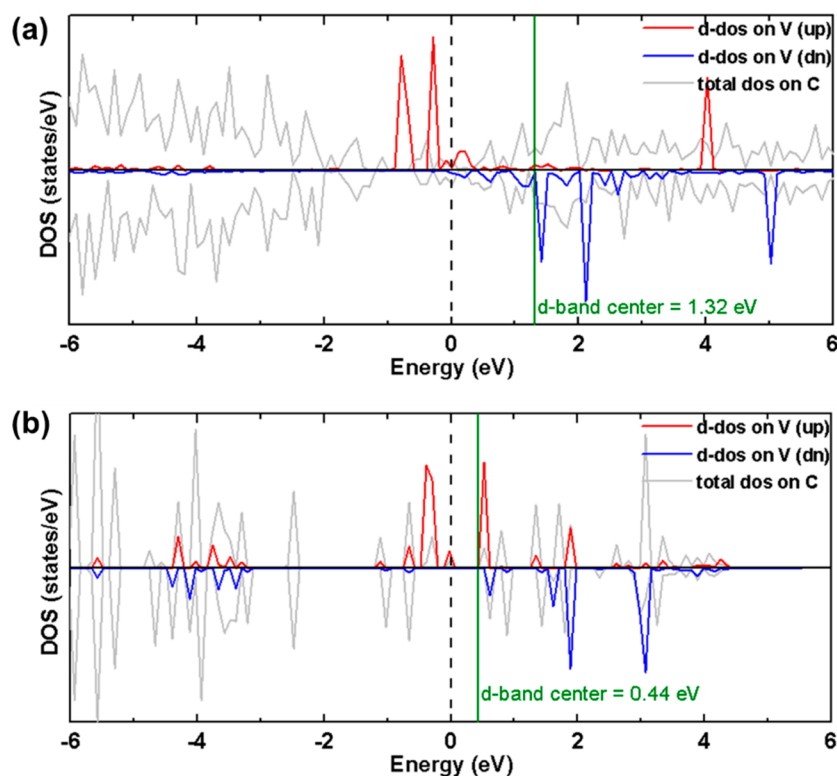


Figure 5. Comparison of local density of states (DOS) of V on N-doped graphene (a) and small nanographene (b). Dashed line denotes E_{Fermi} ; solid green line, the d-band center.

small nanographene than in the 2D graphene. This is also confirmed in the more favorable (negative) formation energies (Table S1). Thus, we demonstrate that the adsorption of hydrogen on metal SACs can be altered by changing the size and dimensionality of the substrate,^{41,42} and is not as solely governed by the local coordination (first coordination shell) of the single atom.²¹ Nonetheless, it is important to note not all SACs experience a downshift in the d-band center when moving from graphene to nanographene; additional descriptors are needed which can capture additional changes to the chemical properties of the active site.

Quantitative Predictions Using Descriptors and Machine Learning. To screen for additional promising catalysts and develop rational design principles, we seek to find viable descriptors which can be used to predict ΔG_{H} . The d-band center is a widely studied descriptor for the interaction of molecules to metal surfaces which has been used extensively for qualitative predictions of energies.^{43,44}

For metal SACs, previous theoretical studies have identified the d-states as being active in adsorption, and attributed to various orbitals such as the d_{xy} and d_{yz} ²³ or the d_z^2 .²² As such, the overall d-band center, or in the case of molecular-like systems, the center of the d-states should provide a good approximation of the position of these d orbitals which in turn determine the position and filling of the M–H antibonding states and the adsorption energy. To test this idea, we calculated the correlation between the d-states center and ΔG_{H} , which turned out to be not great ($R^2 = 0.66$). The low R^2 suggests that other factors beyond the d-band center play a role in determining ΔG_{H} . For example, it has also been shown that the charge transfer between metal and support can be crucial for the catalytic performance of SACs, and a more positive charge on the single atom can lead to a stronger

adsorption of reactant or reaction intermediates such as N_2 , OH, and H.^{23,45–47}

To systematically evaluate the descriptors, we also considered others: the formation energy of the single atom site, the number of filled and unfilled d states near the Fermi level,^{48,49} and atomic properties of the single atom including the ionization potential, electronegativity, d electron count, and the covalent and Zunger d-orbital radii (Table S1).⁵⁰ Then we employed machine-learning regression methods to train models that can predict ΔG_{H} based on the descriptors. Machine learning regression has received increasing attention to provide accurate predictions for complex data sets and chemical phenomena,^{51,52} including chemisorption and catalysis.^{53,54} We compared several commonly used machine learning models: kernel ridge regression, decision trees (random forest), and neural networks (Figure 6a–c). We were able to obtain root mean squared errors (RMSE) of approximately 0.15–0.21 eV in our test set (Table 1), which is quite good given the small set of descriptors and training data and the simplicity of the models used. Additional training data and increasing the complexity of the model could further reduce the testing error.

Relevance and Relationship of Descriptors from Sure Independence Screening and Sparsifying Operator (SISSO). An alternative approach is to create predictive models with human-readable analytical expressions.⁵⁵ Here we used a recently developed and implemented compressed sensing method, SISSO (sure independence screening and sparsifying operator),³⁴ which has been successfully used to provide predictions of adsorption energies on surfaces and other material properties.^{48,49,56} From a list of input descriptors, successive iterations of arithmetic operators are applied to yield analytical expressions of increasing dimen-

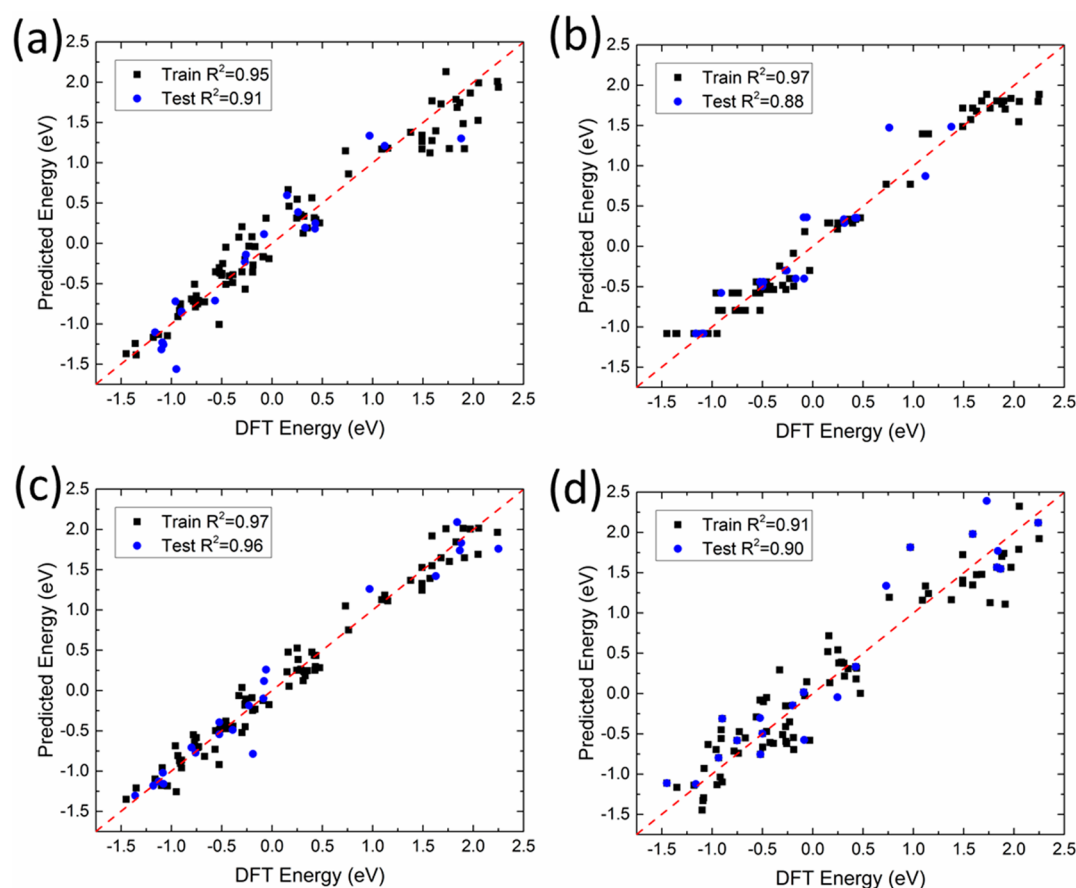


Figure 6. Comparison of DFT calculated versus machine learning predicted ΔG_{H} using (a) kernel ridge regression, (b) random forest regression, (c) neural network regression, and (d) SISSO regression.

Table 1. Performance Comparison of Machine Learning Methods in Predicting ΔG_{H} in Terms of Root-Mean-Squared-Error (RMSE), Mean-Absolute-Error (MAE), and R^2 of Linear Fitting

	training RMSE (eV)	training MAE (eV)	training R^2	test RMSE (eV)	test MAE (eV)	test R^2
kernel ridge	0.240	0.183	0.946	0.261	0.207	0.905
random forest	0.175	0.137	0.973	0.244	0.158	0.881
neural network	0.158	0.123	0.974	0.218	0.149	0.964
SISSO	0.306	0.250	0.913	0.366	0.287	0.903

sional complexity, starting with the Φ_0 feature space and moving on to Φ_1 and higher feature spaces.

We applied SISSO to our data set of 10 input descriptors (Table S1), and after dimension reduction in SISSO, we obtained the highest accuracy with the following expression containing four Φ_1 features:

$$\Delta G_{\text{H}} = -1.032 \times \left(\frac{\epsilon_{\text{d}}}{q} \right) + 13.424 \times \left(\frac{1}{r_{\text{cov}}} \right) + 1.726 \times (\epsilon_{\text{d}} \times \text{EN}) - 0.045 \times (d_{\text{occ}}^2) - 9.241$$

Here the electronegativity (EN), d-states center (ϵ_{d}), covalent radius (r_{cov}), Bader charge (q), and the number of occupied d states (d_{occ}) were selected. This regression yielded a training

RMSE of 0.306 eV and a similar test error of 0.366 eV, indicating a low degree of overfitting (Figure 6d and Table 1). The number of unoccupied d states was not selected in the expression, suggesting a low degree of relevance to hydrogen adsorption, which has a different bonding mechanism compared to methane adsorption, which was previously shown to be highly relevant to the unoccupied states.⁴⁸ Here, feature 4 reveals that more occupied d-states near the Fermi level of the SACs correlate to stronger hydrogen adsorption. Meanwhile features 1 and 3 suggest a competing influence between a positive ϵ_{d} with a large q and a negative ϵ_{d} with a large EN on the adsorption energy. As a consequence, there can be a large spread in ϵ_{d} for a given ΔG_{H} , and close-to-zero ΔG_{H} does not necessarily point to a positive or negative ϵ_{d} .

More complex expressions can be constructed from further iterating the feature space, and while the training errors can be reduced to under 0.20 eV in the Φ_2 and Φ_3 space, the test error remains similar, suggesting the more complex models begin to overfit the data without improvement in predictive ability.

Discussion of the ΔG_{H} Descriptor. Due to the relative simplicity of the HER reaction, the ΔG_{H} is a very general descriptor, working well for many catalysts, including metals,^{37,57} phosphides,⁵⁸ carbides,⁵⁹ nanoclusters,⁶⁰ and SACs.^{22,39} Building upon our predictions, it would be more desirable for a future study to examine the detailed mechanism of HER for the most promising SACs predicted, incorporating

the solvation environment explicitly and also considering the applied potential, as done previously for HER on 1T-MoS₂.⁶¹

CONCLUSIONS

We systematically screened SACs in nitrogen-doped graphene and nanographenes for ΔG_{H} to identify the most promising HER catalysts. In going from graphene to nanographene, we observed a change of hydrogen adsorption on the metals and a corresponding modification in electronic structure, which suggests a useful route for tuning graphene-based SACs by tuning the substrate size. We discovered that the nitrogen-doped nanographene molecules containing V, Rh, and Ir have significantly enhanced HER activity compared to the same SACs on the extended 2D graphene substrate. Further, we employed machine learning to accurately predict ΔG_{H} using various proposed descriptors. Compressed sensing through the SISO method helped select the most relevant descriptors out of the list of candidates and provided an analytical expression for regression that compares favorably with the previous methods. This approach can be used to quickly find better HER catalysts on the basis of further doping and modifying the nanographene substrate, and it can be easily applied to other catalytic reactions as well.

ASSOCIATED CONTENT

Supporting Information

The Supporting Information is available free of charge at <https://pubs.acs.org/doi/10.1021/acs.jpcc.0c04432>.

Values for various descriptors of the single-atom catalysts examined in the text (PDF)

AUTHOR INFORMATION

Corresponding Author

De-en Jiang – Department of Chemistry, University of California, Riverside, California 92521, United States; orcid.org/0000-0001-5167-0731; Email: djiang@ucr.edu

Authors

Victor Fung – Department of Chemistry, University of California, Riverside, California 92521, United States; Center for Nanophase Materials Sciences, Oak Ridge National Laboratory, Oak Ridge, Tennessee 37831, United States; orcid.org/0000-0002-3347-6983

Guoxiang Hu – Department of Chemistry, University of California, Riverside, California 92521, United States; Center for Nanophase Materials Sciences, Oak Ridge National Laboratory, Oak Ridge, Tennessee 37831, United States; orcid.org/0000-0003-2942-8564

Zili Wu – Center for Nanophase Materials Sciences and Chemical Sciences Division, Oak Ridge National Laboratory, Oak Ridge, Tennessee 37831, United States; orcid.org/0000-0002-4468-3240

Complete contact information is available at: <https://pubs.acs.org/doi/10.1021/acs.jpcc.0c04432>

Author Contributions

#V.F. and G.H. contributed equally.

Notes

The authors declare no competing financial interest.

ACKNOWLEDGMENTS

This work was sponsored by the U.S. Department of Energy, Office of Science, Office of Basic Energy Sciences, Chemical Sciences, Geosciences, and Biosciences Division, Catalysis Science Program. This research used resources of the National Energy Research Scientific Computing Center, a DOE Office of Science User Facility supported by the Office of Science of the U.S. Department of Energy under Contract DE-AC02-05CH11231.

REFERENCES

- (1) Lubitz, W.; Tumas, W. Hydrogen: An Overview. *Chem. Rev.* **2007**, *107*, 3900–3903.
- (2) Zheng, Y.; Jiao, Y.; Jaroniec, M.; Qiao, S. Z. Advancing the Electrochemistry of the Hydrogen-evolution Reaction Through Combining Experiment and Theory. *Angew. Chem., Int. Ed.* **2015**, *54*, 52–65.
- (3) Liu, P.; Rodriguez, J. A. Catalysts for Hydrogen Evolution from the [NiFe] Hydrogenase to the Ni₂P (001) Surface: the Importance of Ensemble Effect. *J. Am. Chem. Soc.* **2005**, *127*, 14871–14878.
- (4) Popczun, E. J.; McKone, J. R.; Read, C. G.; Biacchi, A. J.; Wiltrout, A. M.; Lewis, N. S.; Schaak, R. E. Nanostructured Nickel Phosphide as an Electrocatalyst for the Hydrogen Evolution Reaction. *J. Am. Chem. Soc.* **2013**, *135*, 9267–9270.
- (5) Popczun, E. J.; Read, C. G.; Roske, C. W.; Lewis, N. S.; Schaak, R. E. Highly Active Electrocatalysis of the Hydrogen Evolution Reaction by Cobalt Phosphide Nanoparticles. *Angew. Chem., Int. Ed.* **2014**, *53*, 5427–5430.
- (6) Hu, G.; Tang, Q.; Jiang, D.-e. CoP for Hydrogen Evolution: Implications from Hydrogen Adsorption. *Phys. Chem. Chem. Phys.* **2016**, *18*, 23864–23871.
- (7) You, B.; Liu, X.; Hu, G.; Gul, S.; Yano, J.; Jiang, D.-e.; Sun, Y. Universal Surface Engineering of Transition Metals for Superior Electrocatalytic Hydrogen Evolution in Neutral Water. *J. Am. Chem. Soc.* **2017**, *139*, 12283–12290.
- (8) Huang, Z.; Chen, Z.; Chen, Z.; Lv, C.; Meng, H.; Zhang, C. Ni₁₂P₅ Nanoparticles as an Efficient Catalyst for Hydrogen Generation via Electrolysis and Photoelectrolysis. *ACS Nano* **2014**, *8*, 8121–8129.
- (9) Kong, D.; Cha, J. J.; Wang, H.; Lee, H. R.; Cui, Y. First-row Transition Metal Dichalcogenide Catalysts for Hydrogen Evolution Reaction. *Energy Environ. Sci.* **2013**, *6*, 3553–3558.
- (10) Hu, G.; Fung, V.; Sang, X.; Unocic, R. R.; Ganesh, P. Superior Electrocatalytic Hydrogen Evolution at Engineered Non-stoichiometric Two-dimensional Transition Metal Dichalcogenide Edges. *J. Mater. Chem. A* **2019**, *7*, 18357.
- (11) Jaramillo, T. F.; Jørgensen, K. P.; Bonde, J.; Nielsen, J. H.; Horch, S.; Chorkendorff, I. Identification of Active Edge Sites for Electrochemical H₂ Evolution from MoS₂ Nanocatalysts. *Science* **2007**, *317*, 100–102.
- (12) Voiry, D.; Yang, J.; Chhowalla, M. Recent Strategies for Improving the Catalytic Activity of 2D TMD Nanosheets Toward the Hydrogen Evolution Reaction. *Adv. Mater.* **2016**, *28*, 6197–6206.
- (13) Hinnemann, B.; Moses, P. G.; Bonde, J.; Jørgensen, K. P.; Nielsen, J. H.; Horch, S.; Chorkendorff, I.; Nørskov, J. K. Biomimetic Hydrogen Evolution: MoS₂ Nanoparticles as Catalyst for Hydrogen Evolution. *J. Am. Chem. Soc.* **2005**, *127*, 5308–5309.
- (14) Hu, G.; Fung, V.; Sang, X.; Unocic, R. R.; Ganesh, P. Predicting Synthesizable Multi-Functional Edge Reconstructions in Two-dimensional Transition Metal Dichalcogenides. *Npj Comput. Mater.* **2020**, *6*, 1–9.
- (15) Wang, Y.; Mao, J.; Meng, X.; Yu, L.; Deng, D.; Bao, X. Catalysis with Two-Dimensional Materials Confining Single Atoms: Concept, Design, and Applications. *Chem. Rev.* **2019**, *119*, 1806–1854.
- (16) Wang, A.; Li, J.; Zhang, T. Heterogeneous Single-atom Catalysis. *Nat. Rev. Chem.* **2018**, *2*, 65–81.

- (17) Rivera-Cárcamo, C.; Serp, P. Single Atom Catalysts on Carbon-Based Materials. *ChemCatChem* **2018**, *10*, 5058–5091.
- (18) Li, H.; Zhang, H.-x.; Yan, X.-l.; Xu, B.-s.; Guo, J.-j. Carbon-supported Metal Single Atom Catalysts. *New Carbon Materials* **2018**, *33*, 1–11.
- (19) Fei, H.; Dong, J.; Feng, Y.; Allen, C. S.; Wan, C.; Volosskiy, B.; Li, M.; Zhao, Z.; Wang, Y.; Sun, H.; An, P.; Chen, W.; Guo, Z.; Lee, C.; Chen, D.; Shakir, I.; Liu, M.; Hu, T.; Li, Y.; Kirkland, A. I.; Duan, X.; Huang, Y. General Synthesis and Definitive Structural Identification of MN_4C_4 Single-atom Catalysts with Tunable Electrocatalytic Activities. *Nat. Catal.* **2018**, *1*, 63–72.
- (20) Jiang, K.; Siahrostami, S.; Zheng, T.; Hu, Y.; Hwang, S.; Stavitski, E.; Peng, Y.; Dynes, J.; Gangisetty, M.; Su, D.; Attenkofer, K.; Wang, H. Isolated Ni Single Atoms in Graphene Nanosheets for High-performance CO_2 Reduction. *Energy Environ. Sci.* **2018**, *11*, 893–903.
- (21) Xu, H.; Cheng, D.; Cao, D.; Zeng, X. C. A Universal Principle for a Rational Design of Single-atom Electrocatalysts. *Nat. Catal.* **2018**, *1*, 339–348.
- (22) Hossain, M. D.; Liu, Z.; Zhuang, M.; Yan, X.; Xu, G.-L.; Gadre, C. A.; Tyagi, A.; Abidi, I. H.; Sun, C.-J.; Wong, H.; Guda, A.; Hao, Y.; Pan, X.; Amine, K.; Luo, Z. Rational Design of Graphene-Supported Single Atom Catalysts for Hydrogen Evolution Reaction. *Adv. Energy Mater.* **2019**, *9*, 1803689.
- (23) Choi, C.; Back, S.; Kim, N.-Y.; Lim, J.; Kim, Y.-H.; Jung, Y. Suppression of Hydrogen Evolution Reaction in Electrochemical N_2 Reduction Using Single-Atom Catalysts: A Computational Guideline. *ACS Catal.* **2018**, *8*, 7517–7525.
- (24) Zhu, Y.; Peng, W.; Li, Y.; Zhang, G.; Zhang, F.; Fan, X. Modulating the Electronic Structure of Single-Atom Catalysts on 2D Nanomaterials for Enhanced Electrocatalytic Performance. *Small Methods* **2019**, *3*, 1800438.
- (25) Zagal, J. H.; Griveau, S.; Silva, J. F.; Nyokong, T.; Bedioui, F. Metallophthalocyanine-based Molecular Materials as Catalysts for Electrochemical Reactions. *Coord. Chem. Rev.* **2010**, *254*, 2755–2791.
- (26) Costentin, C.; Savéant, J.-M. Towards an Intelligent Design of Molecular Electrocatalysts. *Nat. Rev. Chem.* **2017**, *1*, 0087.
- (27) Fung, V.; Hu, G.; Tao, F. F.; Jiang, D. E. Methane Chemisorption on Oxide-Supported Pt Single Atom. *ChemPhysChem* **2019**, *20*, 2217–2220.
- (28) Kresse, G.; Furthmüller, J. Efficient Iterative Schemes for ab initio Total-energy Calculations Using a Plane-Wave Basis Set. *Phys. Rev. B: Condens. Matter Mater. Phys.* **1996**, *54*, 11169–11186.
- (29) Kresse, G.; Furthmüller, J. Efficiency of ab-initio Total Energy Calculations for Metals and Semiconductors Using a Plane-Wave Basis Set. *Comput. Mater. Sci.* **1996**, *6*, 15–50.
- (30) Perdew, J. P.; Burke, K.; Ernzerhof, M. Generalized Gradient Approximation Made Simple. *Phys. Rev. Lett.* **1996**, *77*, 3865–3868.
- (31) Blöchl, P. E. Projector Augmented-Wave Method. *Phys. Rev. B: Condens. Matter Mater. Phys.* **1994**, *50*, 17953–17979.
- (32) Afeefy, H. Y.; Liebman, J. F.; Stein, S. E. In Neutral Thermochemical Data. *NIST Chemistry WebBook*; Linstrom, P. J., Mallard, W. G., Eds.; NIST Standard Reference Database Number 69; National Institute of Standards and Technology: Gaithersburg, MD, <http://webbook.nist.gov>, (retrieved April, 23, 2020).
- (33) Pedregosa, F.; Varoquaux, G.; Gramfort, A.; Michel, V.; Thirion, B.; Grisel, O.; Blondel, M.; Prettenhofer, P.; Weiss, R.; Dubourg, V. Scikit-learn: Machine learning in Python. *Journal of machine Learning research* **2011**, *12*, 2825–2830.
- (34) Ouyang, R.; Curtarolo, S.; Ahmetcik, E.; Scheffler, M.; Ghiringhelli, L. M. SISSO: A Compressed-sensing Method for Identifying the Best Low-dimensional Descriptor in an Immensity of Offered Candidates. *Physical Review Materials* **2018**, *2*, 083802.
- (35) Erdely-Grúz, T.; Volmer, M. Zur Theorie der Wasserstoff Überspannung. *Z. Phys. Chem.* **1930**, *150A*, 203–213.
- (36) Heyrovský, J. A Theory of Overpotential. *Recl. Trav. Chim. Pays-Bas* **1927**, *46*, 582–585.
- (37) Nørskov, J. K.; Bligaard, T.; Logadottir, A.; Kitchin, J. R.; Chen, J. G.; Pandelov, S.; Stimming, U. Trends in the Exchange Current for Hydrogen Evolution. *J. Electrochem. Soc.* **2005**, *152*, J23–J26.
- (38) Fung, V.; Tao, F.; Jiang, D.-e. Low-Temperature Activation of Methane on Doped Single Atoms: Descriptor and Prediction. *Phys. Chem. Chem. Phys.* **2018**, *20*, 22909–22914.
- (39) Fei, H.; Dong, J.; Arellano-Jiménez, M. J.; Ye, G.; Dong Kim, N.; Samuel, E. L. G.; Peng, Z.; Zhu, Z.; Qin, F.; Bao, J.; Yacaman, M. J.; Ajayan, P. M.; Chen, D.; Tour, J. M. Atomic Cobalt on Nitrogen-doped Graphene for Hydrogen Generation. *Nat. Commun.* **2015**, *6*, 8668.
- (40) Skúlason, E.; Tripkovic, V.; Björketun, M. E.; Gudmundsdóttir, S.; Karlberg, G.; Rossmeisl, J.; Bligaard, T.; Jónsson, H.; Nørskov, J. K. Modeling the Electrochemical Hydrogen Oxidation and Evolution Reactions on the Basis of Density Functional Theory Calculations. *J. Phys. Chem. C* **2010**, *114*, 18182–18197.
- (41) Luo, G.-G.; Zhang, H.-L.; Tao, Y.-W.; Wu, Q.-Y.; Tian, D.; Zhang, Q. Recent Progress in Ligand-centered Homogeneous Electrocatalysts for Hydrogen Evolution Reaction. *Inorg. Chem. Front.* **2019**, *6*, 343–354.
- (42) Tong, L.; Duan, L.; Zhou, A.; Thummel, R. P. First-row Transition Metal Polypyridine Complexes that Catalyze Proton to Hydrogen Reduction. *Coord. Chem. Rev.* **2020**, *402*, 213079.
- (43) Nørskov, J. K.; Bligaard, T.; Rossmeisl, J.; Christensen, C. H. Towards the Computational Design of Solid Catalysts. *Nat. Chem.* **2009**, *1*, 37–46.
- (44) Hammer, B.; Nørskov, J. K. Electronic Factors Determining the Reactivity of Metal Surfaces. *Surf. Sci.* **1995**, *343*, 211–220.
- (45) Chen, Y.; Ji, S.; Zhao, S.; Chen, W.; Dong, J.; Cheong, W.-C.; Shen, R.; Wen, X.; Zheng, L.; Rykov, A. I.; Cai, S.; Tang, H.; Zhuang, Z.; Chen, C.; Peng, Q.; Wang, D.; Li, Y. Enhanced Oxygen Reduction with Single-atomic-site Iron Catalysts for a Zinc-air Battery and Hydrogen-air Fuel Cell. *Nat. Commun.* **2018**, *9*, 5422.
- (46) Back, S.; Lim, J.; Kim, N.-Y.; Kim, Y.-H.; Jung, Y. Single-atom Catalysts for CO_2 Electroreduction with Significant Activity and Selectivity Improvements. *Chem. Sci.* **2017**, *8*, 1090–1096.
- (47) Yang, X.-F.; Wang, A.; Qiao, B.; Li, J.; Liu, J.; Zhang, T. Single-Atom Catalysts: A New Frontier in Heterogeneous Catalysis. *Acc. Chem. Res.* **2013**, *46*, 1740–1748.
- (48) Fung, V.; Hu, G.; Sumpster, B. Electronic Band Contraction Induced Low Temperature Methane Activation on Metal Alloys. *J. Mater. Chem. A* **2020**, *8*, 6057–6066.
- (49) Andersen, M.; Levchenko, S. V.; Scheffler, M.; Reuter, K. Beyond Scaling Relations for the Description of Catalytic Materials. *ACS Catal.* **2019**, *9*, 2752–2759.
- (50) Zunger, A. Systematization of the Stable Crystal Structure of all AB-type Binary Compounds: A Pseudopotential Orbital-radii Approach. *Phys. Rev. B: Condens. Matter Mater. Phys.* **1980**, *22*, 5839–5872.
- (51) Schlexer Lamoureux, P.; Winther, K. T.; Garrido Torres, J. A.; Streibel, V.; Zhao, M.; Bajdich, M.; Abild-Pedersen, F.; Bligaard, T. Machine Learning for Computational Heterogeneous Catalysis. *ChemCatChem* **2019**, *11*, 3581–3601.
- (52) Schleder, G. R.; Padilha, A. C. M.; Acosta, C. M.; Costa, M.; Fazzio, A. From DFT to Machine Learning: Recent Approaches to Materials Science—a Review. *J. Phys.: Materials* **2019**, *2*, 032001.
- (53) Li, Z.; Ma, X.; Xin, H. Feature Engineering of Machine-Learning Chemisorption Models for Catalyst Design. *Catal. Today* **2017**, *280*, 232–238.
- (54) Li, Z.; Wang, S.; Chin, W. S.; Achenie, L. E.; Xin, H. High-throughput Screening of Bimetallic Catalysts Enabled by Machine Learning. *J. Mater. Chem. A* **2017**, *5*, 24131–24138.
- (55) Ghiringhelli, L. M.; Vybiral, J.; Levchenko, S. V.; Draxl, C.; Scheffler, M. Big Data of Materials Science: Critical Role of the Descriptor. *Phys. Rev. Lett.* **2015**, *114*, 105503.
- (56) Xie, S. R.; Stewart, G. R.; Hamlin, J. J.; Hirschfeld, P. J.; Hennig, R. G. Functional Form of the Superconducting Critical Temperature from Machine Learning. *Phys. Rev. B: Condens. Matter Mater. Phys.* **2019**, *100*, 174513.

(57) Greeley, J.; Jaramillo, T. F.; Bonde, J.; Chorkendorff, I.; Nørskov, J. K. Computational High-throughput Screening of Electrocatalytic Materials for Hydrogen Evolution. *Nat. Mater.* **2006**, *5*, 909–913.

(58) Hu, G.; Tang, Q.; Jiang, D.-e. CoP for hydrogen evolution: implications from hydrogen adsorption. *Phys. Chem. Chem. Phys.* **2016**, *18*, 23864–23871.

(59) Zhang, Q.; Jiang, Z.; Tackett, B. M.; Denny, S. R.; Tian, B.; Chen, X.; Wang, B.; Chen, J. G. Trends and Descriptors of Metal-Modified Transition Metal Carbides for Hydrogen Evolution in Alkaline Electrolyte. *ACS Catal.* **2019**, *9*, 2415–2422.

(60) Kwak, K.; Choi, W.; Tang, Q.; Kim, M.; Lee, Y.; Jiang, D.-e.; Lee, D. A Molecule-like PtAu₂₄(SC₆H₁₃)₁₈ Nanocluster as an Electrocatalyst for Hydrogen Production. *Nat. Commun.* **2017**, *8*, 14723.

(61) Tang, Q.; Jiang, D.-e. Mechanism of Hydrogen Evolution Reaction on 1T-MoS₂ from First Principles. *ACS Catal.* **2016**, *6*, 4953–4961.